nature physics

ARTICLES

https://doi.org/10.1038/s41567-018-0272-z

Membrane-induced hydroelastic migration of a particle surfing its own wave

Bhargav Rallabandi[1,4], Naomi Oppenheimer[2,4], Matan Yah Ben Zion[3] and Howard A. Stone[1*]

While coupling between fluid flow and soft elastic surfaces is common in biology and engineering, an analytical description is challenging as it often involves non-linear dynamics. Here we show using theory and experiments that a small particle moving along an elastic membrane through a viscous fluid is repelled from the membrane due to hydroelastic forces. The flow field produces an elastic disturbance in the membrane leading to particle–wave coupling. We derive an analytic expression for the particle trajectory and find that the normal migration velocity of the particle is quadratic in its speed and depends on a combination of the tension and bending resistance of the membrane. Experimentally, we measure the normal displacement of spheres sedimenting under gravity along a suspended elastic membrane and find quantitative agreement with the theoretical predictions with no fitting parameters. We experimentally demonstrate that the effect is strong enough for separation and sorting of particles on the basis of both their size and density. We discuss the significance of our results for particles interacting with biological membranes, and propose the use of our model for membrane elasticity measurements.

Hydrodynamics at low Reynolds number prohibits a net normal force on a spherical particle moving along a rigid wall. Repulsion or attraction of the particle violates time-reversal symmetry. Relaxing the rigidity constraint breaks this symmetry; a rigid sphere moving along a soft wall (or a soft sphere along a rigid wall[1]) experiences a repulsive force. Such forces have been shown to reduce drag near compressed and sheared elastic substrates[2–7]. Here we show that, for a thin membrane of the same material, the effect can be orders of magnitude greater, leading to sizable displacement of suspended particles.

Interactions between cell membranes and surfaces are common in many physiological and cellular processes, including blood flow in capillaries[8–10], filtration in the spleen[11,12], endocytosis[13] and microswimming near interfaces[14–19]. Understanding these hydroelastic interactions on the nano- and microscales is important for efficient drug delivery and release, as they significantly modify the hydrodynamic mobilities of particles such as proteins[20–22]. Recent work has quantified many aspects of particle hydrodynamics near membranes[23–26], but has not addressed non-linear interactions producing repulsive forces.

We develop experiments and theory to demonstrate that a suspended particle translating tangent to a thin elastic membrane (velocity $V_{||}$) through a viscous fluid experiences a significant migration away from the surface (velocity $V_{\perp}$) as a result of fluid-mediated deformations of the membrane. Our experiments comprise spherical particles sedimenting due to gravity near thin elastic sheets suspended under their own weight in silicone oil (details in Methods and Supplementary Information). Figure 1a shows snapshots, at different times, of the trajectory of a sphere near the surface of the sheet (Supplementary Movie online[27]). The sedimentation of the sphere is accompanied by a travelling-wave deformation of the membrane and a migration of the particle away from it, resembling a particle surfing its own wave[28]. As we show, this repulsive migration is a direct consequence of the elasticity of the membrane.

The normal motion is sensitive to the particle size and is strong enough for particle separation and sorting. Figure 2a shows a stroboscopic image of three different-sized particles sedimenting along the elastic sheet. The particles accelerate in the direction of gravity as a consequence of their increasing distance from the sheet over time (resulting in decreasing drag), which appears as an increasing separation distance between consecutive frames. Once settled, the particles are separated and sorted by their size (Fig. 2b): larger and denser particles experience stronger repulsion, settling further from the sheet. These results suggest the possibility of designing size-sorting devices by incorporating flexible structures in fluidic systems.

We develop a theory for the repulsive velocity $V_{\perp}$ of the particle, accounting for hydrodynamic interactions that lead to a small but finite deformation of the elastic membrane. The membrane has a thickness b and bending rigidity B, and is held taut under a tension (force per length) T, which together keep it planar in its undeformed state S_0. The sphere has radius a and translates with velocity $\mathbf{V}=V_{||}\mathbf{e}_y+V_{\perp}\mathbf{e}_z$ as measured in the laboratory reference frame, with a separation distance $h(t)$ that increases with time (Fig. 1). The advective nature of the membrane deformation (Fig. 1a) makes it convenient to describe the fluid-elastic problem in a local cylindrical coordinate system (r, θ, z) whose origin is instantaneously at the point on S_0 closest to the sphere (Fig. 1d), so that S_0 is identified by $z=0$. The fluid flow (velocity $\mathbf{v}$ and stress $\boldsymbol{\sigma}$) excited by the motion of the sphere deforms the membrane to a new position $z=\zeta(\mathbf{r}, t)$, where $\mathbf{r}=(r, \theta)$ is the position vector in the plane S_0.

We consider the limit of small deflections $|\zeta| \ll h$, small separation distances $h \ll a$, and predominantly parallel motion ($V_{||} \gg V_{\perp}$). The Reynolds number in our experiments is small ($\rho_f|\mathbf{V}|a/\mu \leq 0.25$, where ρ_f and μ are the fluid's density and viscosity, respectively), so inertial contributions to either $V_{\perp}$ or $V_{||}$ are negligible (ref. [29] and Supplementary Information). Identifying $\ell = \sqrt{2ah}$ as the length scale over which stresses decay away from the sphere and defining $R=|\mathbf{R}|$ with $\mathbf{R}=\mathbf{r}/\ell$, the fluid pressure acting to deform the membrane is approximately $p^{(0)}=\frac{6\mu V_{||}\ell R\cos\theta}{5h^2(1+R^2)^2}$, produced by the translation of a sphere parallel to a rigid wall at S_0[30]. Then, the membrane defor-

[1]Department of Mechanical and Aerospace Engineering, Princeton University, Princeton, NJ, USA. [2]Center for Computational Biology, Flatiron Institute, Simons Foundation, New York, NY, USA. [3]Center for Soft Matter Research, New York University, New York, NY, USA. [4]These authors contributed equally: Bhargav Rallabandi, Naomi Oppenheimer. *e-mail: hastone@princeton.edu

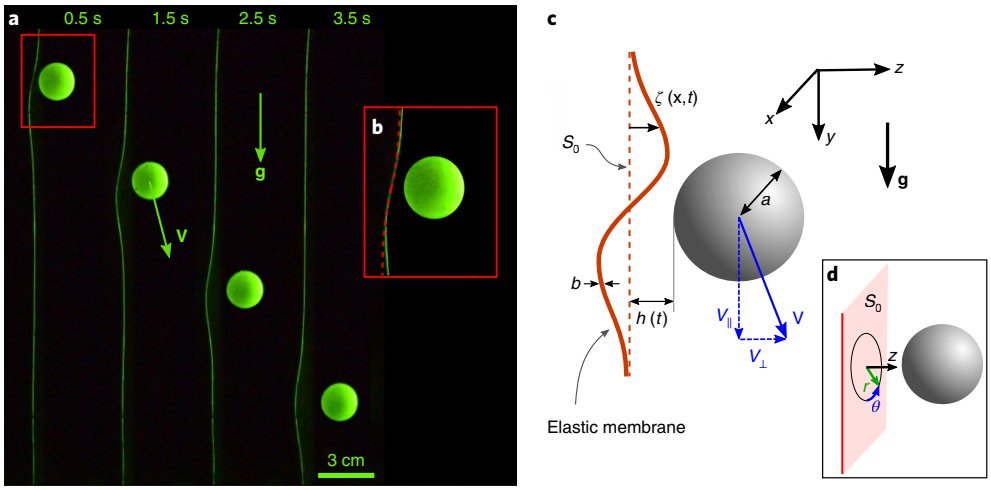

Fig. 1 | Self-surfing and hydroelastic repulsion of a particle near a thin elastic sheet. a, Time sequence showing experimental images of a solid sphere sedimenting under gravity near a vertically suspended rubber sheet in silicone oil. Tracking the position of the sphere at different times after release shows a spontaneous migration away from the sheet. **b**, Close-up showing the shape of the sheet and the theoretical prediction of equations (1a) and (1b) (red dashed curve) on the centre plane ($\theta = \{0, \pi\}$) with no fitting parameters; the maximum deformation amplitude is about 2 mm in both the theory and the experiments. **c**, Sketch of the system indicating the coordinate system and relevant parameters. The dashed line indicates the undeformed position S_0 ($z = 0$) of the elastic membrane. **d**, The local coordinate system (r, θ, z) that we use to describe the hydroelastic problem near the particle.

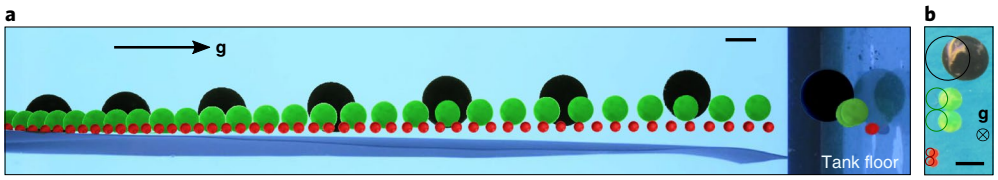

Fig. 2 | Size-dependent sorting of spherical particles sedimenting near an elastic membrane. a, Overlaid stroboscopic images, taken at fixed intervals of 0.33 s, indicating the motion of three different particles (all Delrin, with radii 1.5 mm (red), 4 mm (green) and 8 mm (black)). **a**,**b**, Final resting positions of the particles on the floor of the tank as viewed from the side (**a**) or from above (**b**), showing that the particles are sorted by their size at the end of their fall. All particles are released at the top of the tank with the same initial surface-to-surface separation distance from the sheet; initial positions are indicated as circular outlines in **b**. The scale bar is 1 cm in both panels.

mation ζ is governed by the stress balance, $p^{(0)} = -(B\nabla^4 - T\nabla^2)\zeta$[31–33]. Introducing a two-dimensional wave-vector $\mathbf{k}$ with a polar representation (k, φ), the deformation can be expressed in Fourier space [$\hat{f}(\mathbf{k}) = \int_{\mathbb{R}^2} f(\mathbf{R})^{-\mathbf{k}\cdot\mathbf{R}} \mathrm{d}^2\mathbf{R}$, with $\mathbf{k}\cdot\mathbf{R} = kR\cos(\varphi - \theta)$], as

$$\hat{\zeta}(\mathbf{k}) = \frac{6\pi i \Lambda k a H}{5(k^4 + \tau H k^2)} K_0(k)\cos\varphi, \quad \text{with} \tag{1a}$$

$$\Lambda = \frac{4\sqrt{2}\,\mu V_{\|} a^2}{BH^{1/2}}, \quad H = \frac{h}{a} \quad \text{and} \quad \tau = \frac{2Ta^2}{B} \tag{1b}$$

Here, K_0 is the order-zero modified Bessel function of the second kind, $\Lambda = O(|\zeta|/h)$ is the small deformation amplitude relative to the gap height, τ is a dimensionless tension and H is the dimensionless separation distance, which varies in time. The inverse transform of equation (1a), evaluated numerically, yields the membrane shape $\zeta(\mathbf{r})$, shown in Fig. 1b with no adjustable parameters.

The deformed membrane perturbs the lubrication pressure ($p = p^{(0)} + \Lambda p^{(1)} + \ldots$), which results in a normal velocity of the particle $V_\perp$. We calculate $V_\perp$ using the Lorentz reciprocal theorem for viscous flows[34], which often provides a useful tool to evaluate hydrodynamic interactions in systems with deformable boundaries[35,36]. In the quasi-steady limit and for small deformations (see Methods), we find

$$V_\perp = \frac{h}{6\pi\mu a^2 V'} \int_{S_0} (V_{||} p'(\cos\theta)\partial_r - \mu\ \partial_z \mathbf{v}' \cdot \partial_z \mathbf{v}^{(0)})\zeta\ \mathrm{d}^2\mathbf{r} \tag{2}$$

where $\mathbf{v}^{(0)}(\mathbf{r})$ is the fluid velocity associated with $p^{(0)}$ and primed quantities refer to the flow around a sphere translating normal to a rigid plane at S_0.

We evaluate the integral (2) in Fourier space by applying Parseval's identity and using known results from lubrication theory (see Methods). Utilizing expression (1b) for $\hat{\zeta}(\mathbf{k})$, we obtain

$$V_\perp = \frac{3\mu a^2 V_{||}^2}{25B} \mathcal{F}(\tau H), \quad \text{where} \tag{3a}$$

$$\mathcal{F}(\tau H) = \int_0^\infty \frac{2k^4 K_0^2(k)}{k^4 + \tau H k^2} k\ \mathrm{d}k \tag{3b}$$

as our main result for the normal migration velocity of the particle. The positive-definite function $\mathcal{F}(\tau H)$ decays monotonically from

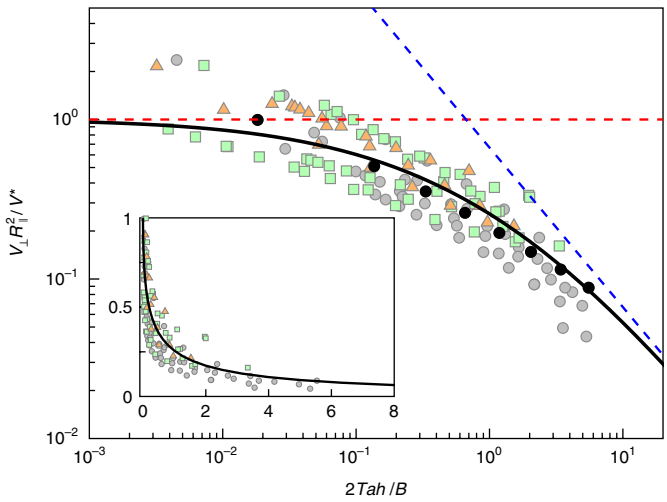

Fig. 3 | Comparison of the experimental results with the theory. Rescaled normal velocity $V_\perp \mathcal{R}_\parallel^2(H)/V^*$ versus the dimensionless tension $\tau H = 2Tah/B$, showing the theoretical prediction $\mathcal{F}(\tau H)$ (equations (3a), (3b) and (4)) as a solid black curve with asymptotes indicated as dashed lines. Experimental data for several parameter combinations (circles, 0.25 mm; squares, 0.38 mm; triangles, 0.5 mm thick sheets) are in agreement with the theoretical prediction. Each set of symbols represents data for several different sphere radii and densities. Since h increases with time, each sphere samples a range of $2Tah/B$ values over its trajectory. The black circles indicate one such trajectory (glass sphere, $a = 5$ mm; $b = 0.25$ mm), where the value of $2Tah/B$ is initially small (due to small h; bending dominates) and decreases over the course of the motion (tension dominates). The inset shows the same data on a graph with linear axes.

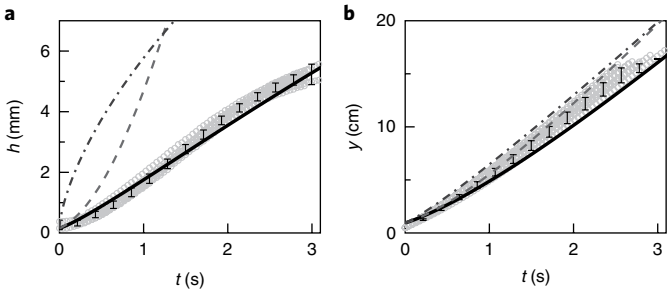

Fig. 4 | Typical trajectory of a sphere. a, Normal displacement $h(t)$. **b**, Tangential displacement $y(t)$. Symbols are experimental measurements (error bars indicate 1 s.d.) for a 5 mm radius glass sphere and a 0.38 mm thick sheet, and the solid lines correspond to theoretical predictions accounting for bending and tension. Bending-dominated (dashed) and tension-dominated (dash-dotted) limits are indicated for comparison.

unity ($\tau H \ll 1$; bending dominates) to $\frac{2}{3\tau H}$ ($\tau H \gg 1$, tension dominates) as shown in Fig. 3; we note that $\mathcal{F}$ can be expressed in terms of special functions (see Methods). Thus, the sphere experiences a repulsive normal velocity $V_\perp$ that is quadratic in its speed $V_\parallel$ along the membrane. This quadratic dependence breaks kinematic reversibility, that is, the sphere migrates away from the sheet irrespective of the direction of its tangential motion. The repulsive migration for thin sheets is consistent with previous studies reporting lift forces near soft substrates[3,4], although here it is several orders of magnitude greater (for examples see Supplementary Information). The physical mechanism for the migration can be understood based on the viscous lubrication principle that fluid flow from wide openings to narrow ones creates a positive pressure and so produces $V_\perp > 0$ (see Supplementary Information for a detailed discussion).

In our experiments, the driving force is gravity, which is balanced by a viscous drag to establish $V_\parallel = 2a^2 g(\Delta\rho_p)/(9\mu\mathcal{R}_\parallel)$, where $\Delta\rho_p = \rho_p - \rho_f$. The dimensionless resistance to tangential motion, $\mathcal{R}_\parallel(H)$, can be approximated by its limiting form for translation along a rigid plane, provided in ref. [37]. Substituting the above expression for $V_\parallel$ into equation (3a) yields

$$V_\perp = V^* \frac{\mathcal{F}(\tau H)}{\mathcal{R}_\parallel^2(H)} \quad \text{with} \quad V^* = \frac{4a^6 g^2 (\Delta\rho_p)^2}{675\mu B} \tag{4}$$

Note that the relative importance of tension to bending resistance in $V_\perp$ is quantified by the dimensionless parameter $\tau H = \frac{2Tah}{B}$. Since H increases with time, this ratio is not constant during the motion of a particle, so that either tension or bending may dominate during different parts of the trajectory.

The displacements $y(t)$ and $h(t)$ for different combinations of sphere and sheet properties are obtained from image analysis. We find that the normal velocity $V_\perp$ depends strongly on the properties of both the sheet and the sphere, and is always smaller than the sedimentation velocity $V_\parallel$ (Fig. 4). Although the sheet tension decreases in the direction of gravity, we approximate it by its mean value and use $T = \frac{1}{2}(\Delta\rho_s) gLb$, where $\Delta\rho_s = \rho_f - \rho_s$, to compare the experimental data with our theoretical predictions; relaxing this simplification yields only minor differences (see Supplementary Information). Thus, $\tau = \frac{gLa^2(\Delta\rho_s)}{B} = \frac{12(1-\nu^2)gL(\Delta\rho_s)}{E(b/a)^2}$ (compare equation (1b)), where $\nu \approx 0.48$ is the Poisson ratio and E is the Young's modulus of the sheet. τ is greater for thinner sheets and larger particles, and is in the range 0.25–8 in our experiments. Recalling that the relative magnitudes of tension and bending are determined by τH (see for example equation (4)), we expect bending to be important at small separation distances $\tau H \ll 1$, and for tension to dominate for larger separation distances with $\tau H \gg 1$; our experimental data span both of these limiting regimes and are in good agreement with the theoretical prediction (Fig. 3).

We compute the trajectory ($y(t)$, $h(t)$) by numerically integrating the velocity components, $V_\perp$ (equation (4)) and $V_\parallel$. Figure 4 shows the trajectory of a sphere with a particular combination of sheet and particle properties. The theoretical predictions for the displacement, without adjustable parameters, are plotted as solid lines, showing that both bending (dashed) and tension (dash–dotted) contributions must be incorporated to achieve quantitative agreement with the experimentally measured trajectories (grey circles).

The system transitions between bending- and tension-dominated regimes as the separation distance increases over time. This transition is indicated for a single trajectory (black circles in Fig. 3), but is clearly observed when varying system parameters such as particle size and density as well as the sheet bending rigidity, as shown in Fig. 3.

Neglecting the weak (logarithmic) dependence of $V_\parallel$ on H, the normal velocity is constant in the bending-dominated regime ($H \ll \tau^{-1}$), that is, the separation distance increases linearly with time, $h \approx \frac{3\mu a^2 V_\parallel^2}{25B} t$ for sufficiently small h. In our experiments, we do not observe trajectories that are characterized by bending alone, although bending is likely to dominate for smaller particles (since $\tau \propto a^2$). In the tension-dominated limit ($\tau H \gg 1$; long times or thin sheets), integrating equations (3a) and (3b) yields $h \approx \sqrt{2\mu a t/(25T)}\, V_\parallel$, again neglecting the dependence of $V_\parallel$ on H. For our gravity-driven experiments, this expression reduces to $h \approx h^* \sqrt{x/L}$, where $h^* = \frac{2\sqrt{2}}{15}\left(\frac{\Delta\rho_p}{\Delta\rho_s}\right)^{\frac{1}{2}} a^{\frac{3}{2}} b^{-\frac{1}{2}}$. We find a good collapse of the measured trajectories for different particle sizes, as indi-

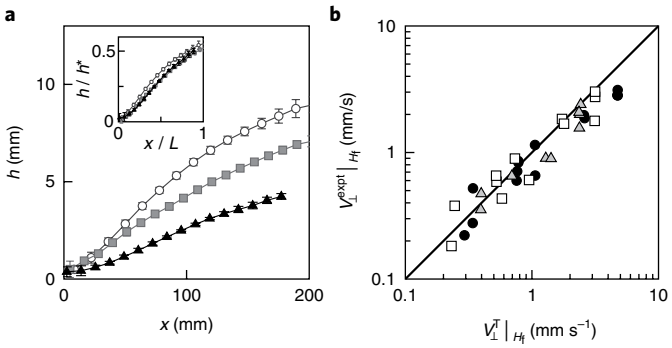

Fig. 5 | The normal migration depends on the size and the density of the particles, as well as the properties of the sheet. a, Experimental trajectories of three different spheres (circles, glass, $a_p = 5$ mm; squares, glass, $a_p = 3$ mm; triangles, Delrin, $a_p = 6$ mm) near a sheet of thickness $b = 0.25$ mm. Inset, rescaled trajectories for tension-dominated dynamics as discussed in the text. Error bars indicate 1 s.d. **b**, By the end of their trajectories ($H = H_f$), the normal velocity is dominated by tension; measured velocities (symbols) are plotted against the tension-dominated theoretical prediction, $V_\perp^T|_{H_f} = \frac{4a^4g^2(\Delta\rho_p)^2}{2,025\mu T H_f \mathcal{R}_{||}^2(H_f)}$. The data span all sheet thicknesses (circles, $b = 0.25$ mm; squares, $b = 0.38$ mm; triangles, $b = 0.5$ mm) and sphere properties (not indicated).

cated in Fig. 5a. For all the experiments, we can extract data points where the system is tension dominated. In particular, the measured $V_\perp$ of each particle at the end of its trajectory (for which particles assume final separation distances $H = H_f$) is well described by the tension-dominated limit of the theory, $V_\perp^T|_{H_f} = \frac{4a^4g^2(\Delta\rho_p)^2}{2,025\mu T}\frac{1}{H_f\mathcal{R}_{||}(H_f)}$, as shown in Fig. 5b.

We comment on extensions of the theoretical framework developed here. It is possible to include a confining potential G (a force per volume), such that the membrane deformation is governed by $p^{(0)} = -(B\nabla^4 + T\nabla^2 + G)\zeta$. Such a confining potential may be externally applied using an optical trap[38], or for biological membranes can arise from a non-zero curvature[33], finite system size or an underlying cytoskeleton[23,39]. In macroscopic systems, such a potential often results from a body force, such as gravity, acting normal to the membrane. The effect of this added potential to the normal velocity $V_\perp$ is accounted for by modifying the denominator of equations (3a) and (3b) to $(k^4 + \tau Hk^2 + \gamma H^2)$, where $\gamma = G\ell^4 / (BH^2) = 4Ga^4/B$. For a cylindrical object translating perpendicular to its axis (here the x axis, compare Fig. 1b), the only modification to $V_\perp$ involves replacing $K_0(k)$ by $\frac{5}{3}\sqrt{\frac{2}{k}}\,e^{-k}$ in equations (3a) and (3b); the results of refs [3,4] then correspond to the limit $\gamma \gg 1$ (Methods). Finally, we note that the mechanism for hydroelastic migration and the scaling laws obtained here persist for active particles (for example microswimmers), but with modified prefactors that depend on the details of the propulsion mechanism. In particular, a fore–aft pressure asymmetry due to the motion of active particles[40] is sufficient to induce migration (see Supplementary Information).

We have demonstrated theoretically and experimentally that a particle moving along a membrane will experience a hydroelastic repulsion. There are several consequences of this effect. (1) A swimming bacterium ($\approx 1\,\mu$m) near a membrane $B \approx 10 k_B \mathcal{T}$ ($\mathcal{T}$ denotes temperature) with a typical speed ($\approx 30\,\mu$m s^{-1}) can be hydroelastically repelled at a speed that is comparable to its own. (2) The repulsive migration of a microswimmer propelled near a bio-membrane is expected to be several orders of magnitude greater than the lift generated by a compressible substrate (such as the cytoskeleton, $G \approx 10$–1000 Pa). On macroscopic scales, the particles in our experiments experience a force greater by about three orders of magnitude than they would in a comparable experiment with a soft substrate (refs [4,5,7]; Supplementary Information). (3) Our model suggests the possibility of a non-intrusive measurement of the elastic properties of biological membranes, one that does not require thermal equilibrium (for example by using a micrometre-sized bead and optical or magnetic tweezers[41,42]). (4) Small thermal fluctuations of a bio-membrane result in a reduced effective bending rigidity[43,44] and are therefore expected to enhance the repulsive migration due to hydroelastic surfing (Supplementary Information) (though shear may suppress such fluctuations[45]). (5) Our macroscopic sedimentation experiments show that the hydroelastic repulsion is sensitive enough to the size of the particle for sorting and separation purposes. This large number of possibilities suggests new opportunities for experiments and theory that take advantage of hydroeleastic lift generated by flexible sheets.

Online content

Any methods, additional references, Nature Research reporting summaries, source data, statements of data availability and associated accession codes are available at https://doi.org/10.1038/s41567-018-0272-z.

Received: 19 March 2018; Accepted: 1 August 2018;
Published online: 17 September 2018

References

1. Abkarian, M., Lartigue, C. & Viallat, A. Tank treading and unbinding of deformable vesicles in shear flow: determination of the lift force. *Phys. Rev. Lett.* **88**, 068103 (2002).
2. Coyle, D. J. Forward roll coating with deformable rolls: a simple one-dimensional elastohydrodynamic model. *Chem. Eng. Sci.* **43**, 2673–2684 (1988).
3. Sekimoto, K. & Leibler, L. A mechanism for shear thickening of polymer-bearing surfaces: elasto-hydrodynamic coupling. *Europhys. Lett.* **23**, 113 (1993).
4. Skotheim, J. M. & Mahadevan, L. Soft lubrication. *Phys. Rev. Lett.* **92**, 245509 (2004).
5. Skotheim, J. M. & Mahadevan, L. Soft lubrication: the elastohydrodynamics of nonconforming and conforming contacts. *Phys. Fluids* **17**, 092101 (2005).
6. Snoeijer, J. H., Eggers, J. & Venner, C. H. Similarity theory of lubricated Hertzian contacts. *Phys. Fluids* **25**, 101705 (2013).
7. Saintyves, B., Jules, T., Salez, T. & Mahadevan, L. Self-sustained lift and low friction via soft lubrication. *Proc. Natl Acad. Sci. USA* **113**, 5847–5849 (2016).
8. Secomb, T. W., Skalak, R., Özkaya, N. & Gross, J. Flow of axisymmetric red blood cells in narrow capillaries. *J. Fluid. Mech.* **163**, 405–423 (1986).
9. Noguchi, H. & Gompper, G. Shape transitions of fluid vesicles and red blood cells in capillary flows. *Proc. Natl Acad. Sci. USA* **102**, 14159–14164 (2005).
10. Dzwinel, W., Boryczko, K. & A, Y. D. A discrete-particle model of blood dynamics in capillary vessels. *J. Colloid Interface. Sci.* **258**, 163–173 (2003).
11. Jandl, J. H., Greenberg, M., Yonemoto, R. & Castle, W. Clinical determination of the sites of red cell sequestration in hemolytic anemias. *J. Clin. Invest.* **35**, 842–867 (1956).
12. Pivkin, I. V. et al. Biomechanics of red blood cells in human spleen and consequences for physiology and disease. *Proc. Natl Acad. Sci. USA* **113**, 7804–7809 (2016).
13. Goldstein, J. L., Anderson, R. G. W. & Brown, M. S. Coated pits, coated vesicles, and receptor-mediated endocytosis. *Nature* **279**, 679–685 (1979).
14. Trouilloud, R., Tony, S. Y., Hosoi, A. E. & Lauga, E. Soft swimming: exploiting deformable interfaces for low Reynolds number locomotion. *Phys. Rev. Lett.* **101**, 048102 (2008).
15. Giacché, D., Ishikawa, T. & Yamaguchi, T. Hydrodynamic entrapment of bacteria swimming near a solid surface. *Phys. Rev. E* **82**, 056309 (2010).
16. Dias, M. A. & Powers, T. R. Swimming near deformable membranes at low Reynolds number. *Phys. Fluids* **25**, 101901 (2013).
17. Ledesma-Aguilar, R. & Yeomans, J. M. Enhanced motility of a microswimmer in rigid and elastic confinement. *Phys. Rev. Lett.* **111**, 138101 (2013).
18. Boryshpolets, S. et al. Different swimming behaviors of sterlet (*Acipenser ruthenus*) spermatozoa close to solid and free surfaces. *Theriogenology* **79**, 81–86 (2013).
19. Lushi, E., Wioland, H. & Goldstein, R. E. Fluid flows created by swimming bacteria drive self-organization in confined suspensions. *Proc. Natl Acad. Sci. USA* **111**, 9733–9738 (2014).
20. Lodish, H *et al. Molecular Cell Biology* 3rd edn (Scientific American Books, New York, NY, 1995).

21. Fradin, C., Abu-Arish, A., Granek, R. & Elbaum, M. Fluorescence correlation spectroscopy close to a fluctuating membrane. *Biophys. J.* **84**, 2005–2020 (2003).
22. Kimura, Y., Mori, T., Yamamoto, A. & Mizuno, D. Hierarchical transport of nanoparticles in a lyotropic lamellar phase. *J. Phys. Condens. Matter* **17**, S2937 (2005).
23. Bickel, T. Brownian motion near a liquid-like membrane. *Eur. Phys. J. E* **20**, 379–385 (2006).
24. Bickel, T. Hindered mobility of a particle near a soft interface. *Phys. Rev. E* **75**, 041403 (2007).
25. Daddi-Moussa-Ider, A., Lisicki, M. & Gekle, S. Mobility of an axisymmetric particle near an elastic interface. *J. Fluid. Mech.* **811**, 210–233 (2017).
26. Daddi-Moussa-Ider, A. & Gekle, S. Hydrodynamic mobility of a solid particle near a spherical elastic membrane: axisymmetric motion. *Phys. Rev. E* **95**, 013108 (2017).
27. Rallabandi, B., Oppenheimer, N., Zion, M. Y. B. & Stone, H. A. Membrane induced hydroelastic migration of a particle surfing its own wave. *figshare* https://figshare.com/articles/All_Figure_Data/6030572/9 (2018).
28. Bush, J. W. M. Pilot-wave hydrodynamics. *Annu. Rev. Fluid Mech.* **47**, 269–292 (2015).
29. Becker, L. E., McKinley, G. H. & Stone, H. A. Sedimentation of a sphere near a plane wall: weak non-Newtonian and inertial effects. *J. Non-Newtonian Fluid Mech.* **63**, 201–233 (1996).
30. O'Neill, M. E. & Stewartson, K. On the slow motion of a sphere parallel to a nearby plane wall. *J. Fluid. Mech.* **27**, 705–724 (1967).
31. Landau, L. D., & Lifshitz, E. M. *Theory of Elasticity. Volume 7 of Course of Theoretical Physics* (Elsevier, New York, NY, 1986).
32. Helfrich, W. Elastic properties of lipid bilayers: theory and possible experiments. *Z. Naturforsch. C* **28**, 693–703 (1973).
33. Seifert, U. Configurations of fluid membranes and vesicles. *Adv. Phys.* **46**, 13–137 (1997).
34. Happel, J. & Brenner, H. *Low Reynolds Number Hydrodynamics with Special Application to Particulate Media* (Prentice-Hall, The Hague, 1965).
35. Berdan, C. II & Leal, L. G. Motion of a sphere in the presence of a deformable interface: I. Perturbation of the interface from flat: the effects on drag and torque. *J. Colloid Interface Sci.* **87**, 62–80 (1982).
36. Yang, S.-M. & Leal, L. G. Motions of a fluid drop near a deformable interface. *Int. J. Multiph. Flow* **16**, 597–616 (1990).
37. Goldman, A. J., Cox, R. G. & Brenner, H. Slow viscous motion of a sphere parallel to a plane wall—I Motion through a quiescent fluid. *Chem. Eng. Sci.* **22**, 637–651 (1967).
38. Verhoeff, A. A., Lavergne, F. A., Bartolo, D., Aarts, D. G. A. L. & Dullens, R. P. A. Optical trapping of interfaces at ultra-low interfacial tension. *Soft Matter* **11**, 3100–3104 (2015).
39. Fournier, J.-B., Lacoste, D. & Raphaël, E. Fluctuation spectrum of fluid membranes coupled to an elastic meshwork: jump of the effective surface tension at the mesh size. *Phys. Rev. Lett.* **92**, 018102 (2004).
40. Spagnolie, S. E. & Lauga, E. Hydrodynamics of self-propulsion near a boundary: predictions and accuracy of far-field approximations. *J. Fluid. Mech.* **700**, 105–147 (2012).
41. Shlomovitz, R., Evans, A. A., Boatwright, T., Dennin, M. & Levine, A. J. Measurement of monolayer viscosity using noncontact microrheology. *Phys. Rev. Lett.* **110**, 137802 (2013).
42. Boatwright, T., Dennin, M., Shlomovitz, R., Evans, A. A. & Levine, A. J. Probing interfacial dynamics and mechanics using submerged particle microrheology. II. Experiment. *Phys. Fluids* **26**, 071904 (2014).
43. Peliti, L. & Leibler, S. Effects of thermal fluctuations on systems with small surface tension. *Phys. Rev. Lett.* **54**, 1690 (1985).
44. Nelson, D. & Peliti, L. Fluctuations in membranes with crystalline and hexatic order. *J. Phys. (Paris)* **48**, 1085–1092 (1987).
45. Derks, D., Aarts, D. G. A. L., Bonn, D., Lekkerkerker, H. N. W. & Imhof, A. Suppression of thermally excited capillary waves by shear flow. *Phys. Rev. Lett.* **97**, 038301 (2006).

Acknowledgements

The authors acknowledge support from the National Science Foundation via award DMS-1614907, and partial support from the Carbon Mitigation Initiative of Princeton University. M.Y.B.Z. acknowledges support by the Center for Bio Inspired Energy Sciences, an Energy Frontier Research Center funded by the DOE, Office of Sciences, Basic Energy Sciences, under award DE-SC0000989 (Paul M. Chakin). We thank T. Salez for preliminary discussions, M. Shelley for helpful ideas and J. Nunes, A. Perazzo and Y. E. Yu for their help with the experiments.

Author contributions

B.R. and N.O. contributed equally to this work. B.R., N.O. and H.A.S conceived the project and developed the theory. B.R., N.O. and M.Y.B.Z. performed the experiments. All authors analysed and interpreted the data and wrote the paper.

Competing interests

The authors declare no competing interests.

Additional information

Supplementary information is available for this paper at https://doi.org/10.1038/s41567-018-0272-z.

Reprints and permissions information is available at www.nature.com/reprints.

Correspondence and requests for materials should be addressed to H.A.S.

Publisher's note: Springer Nature remains neutral with regard to jurisdictional claims in published maps and institutional affiliations.

Methods

Theoretical derivation. To calculate the normal velocity, equations (3a) and (3b), we use the Lorentz reciprocal theorem $\int_S \mathbf{n}\cdot\boldsymbol{\sigma}\cdot\mathbf{v}'\mathrm{d}^2\mathbf{r} = \int_S \mathbf{n}\cdot\boldsymbol{\sigma}'\cdot\mathbf{v}\mathrm{d}^2\mathbf{r}$, where $\mathbf{v}'$ and $\boldsymbol{\sigma}'$ are the known fluid velocity and stress fields around a sphere moving perpendicular to a *rigid* wall, and $\mathbf{n}$ is the unit normal to the surface. The integration is over the *undeformed* bounding surface of the fluid domain S, which comprises S_0, the particle surface S_p and a surface at infinity S_∞. With the conditions $\mathbf{v}=\mathbf{v}'=\mathbf{0}$ on S_p (no-slip), and $\mathbf{v}=-\mathbf{V}$ (and $\mathbf{v}'=-\mathbf{V}'$) on S_∞, the reciprocal relation becomes $F'_\perp V_\perp = \int_{S_0}\mathbf{n}\cdot\boldsymbol{\sigma}'\cdot(\mathbf{v}+V)\mathrm{d}^2\mathbf{r}$, where $F'_\perp$ is the applied force on the sphere in the auxiliary (primed) problem[46].

To obtain $\mathbf{v}$ on S_0 ($z=0$), we use the no-slip condition $\mathbf{v}|_{z=\zeta} = -\mathbf{V} - \mathbf{e}_z V_{||}\partial_y\zeta$, where we have assumed a quasi-static membrane deformation in the particle reference frame ($|\partial_t\zeta| \ll V_{||}\,|\partial_y\zeta|$). We map this boundary condition onto the plane S_0 by means of a Taylor expansion, $\mathbf{v}|_{S_0} \approx \mathbf{v}|_{z=\zeta} - \zeta\partial_z\mathbf{v}|_{S_0} = -\mathbf{V} - \mathbf{e}_z V_{||}\partial_y\zeta - \zeta\partial_z\mathbf{v}|_{S_0}$. Next, we approximate the velocity gradient by that of the zeroth-order problem (translation parallel to a planar wall), $\partial_z\mathbf{v} \approx \partial_z\mathbf{v}^{(0)}$. Recognizing that the applied force on the sphere in the auxiliary problem is $F' = 6\pi\mu a^2 V'/h$ in the lubrication limit yields equation (2). We then use standard results from lubrication theory[30,46]: $p' = -\frac{3\mu V'\ell^2}{2h^3(1+R^2)^2}$, $\partial_z\mathbf{v}'|_{z=0} = -\frac{3V'\ell R}{h^2(1+R^2)^2}\mathbf{e}_r$ and $\partial_z\mathbf{v}^{(0)}|_{z=0} = \frac{2V_{||}}{5h(1+R^2)}\left\{\left(7-\frac{6}{1+R^2}\right)\cos\theta - \sin\theta\right\}$. Evaluating the resulting definite integral in Fourier space finally results in (3a) and (3b). The result can be expressed in terms of known functions as

$$V_\perp = \frac{3\mu a^2 V_{||}^2}{25B}\mathcal{F}(\tau H), \quad \text{with} \tag{5a}$$

$$\mathcal{F}(\tau H) \equiv \int_0^\infty \frac{2k^4 K_0^2(k)}{k^4+\tau H k^2} k\,\mathrm{d}k \tag{5b}$$

$$= \frac{\sqrt{\pi}}{2} MeijerG^{4,1}_{2,4}\left(\tau H \,\middle|\, \begin{matrix} 0, \frac{3}{2} \\ 0,1,1,1 \end{matrix}\right). \tag{5c}$$

As noted in the main text, for $\tau H \ll 1$, that is the bending-dominated limit, equation (5b) gives $\mathcal{F}=1$. In the opposite, tension-dominated limit, $\tau H \gg 1$, equation (5b) gives $\mathcal{F} = \frac{2}{3\tau H}$.

For a cylinder translating tangent to the membrane, the normal velocity is

$$V_\perp^{\mathrm{cyl}} = \frac{2\mu a^2 V_{||}^2}{3B}\mathcal{F}^{\mathrm{cyl}}(\tau H), \quad \text{with} \tag{6a}$$

$$\begin{aligned}\mathcal{F}^{\mathrm{cyl}}(\tau H) \;=\; & \int_0^\infty \frac{2k^4 \mathrm{e}^{-2k}}{k^4+\tau H k^2}\mathrm{d}k = 1 - \sqrt{\tau H}\,[\pi\cos(2\sqrt{\tau H})] \\ & -2\,\mathrm{Ci}(2\sqrt{\tau H})\sin(2\sqrt{\tau H}) \\ & [+2\,\mathrm{Si}(2\sqrt{\tau H})\cos(\sqrt{\tau H})]\end{aligned} \tag{6b}$$

where Ci and Si are cosine and sine integrals, respectively.

Conversely, if the sphere is forced to translate parallel to the soft membrane without normal migration (by the application of an external normal force), it will experience a counterbalancing repulsive hydrodynamic force $F_\perp^{\mathrm{H}} = 6\pi\mu V_\perp a^2/h$. Similarly, a cylinder forced to translate tangent to the soft membrane experiences a repulsive force per unit length

$$f_\perp^{\mathrm{H,cyl}} = 3\sqrt{2}\pi\mu V_\perp^{\mathrm{cyl}}\left(\frac{a}{h}\right)^{3/2} = \frac{2\sqrt{2}\pi\mu^2 a^{7/2} V_{||}^2}{Bh^{3/2}}\mathcal{F}^{\mathrm{cyl}}(\tau H) \tag{7}$$

Experimental details. Our experimental setup consists of a tank (16 cm × 16 cm × 30 cm) containing silicone oil (density 0.97 g cm^{-3}, viscosity 1 Pa s; Sigma Aldrich); see an image of the setup in Supplementary Information. Silicone rubber sheets (Marian; Shore A durometer 10) of size 8 cm × 30 cm, density $\rho_s = 1.1$ g cm^{-3} and thicknesses b (0.25, 0.38, 0.5 mm) are suspended close to the middle of the container such that their top end is held fixed and their bottom end is free. The immersed length of the sheets in the oil is $L = 20$ cm. Being denser than the fluid, the sheets are suspended under their own weight, which provides tension T in the range 0.03–0.06 N m^{-1}.

We use a linear extension experiment to measure the Young's modulus of each sheet by suspending it in air and progressively loading (and subsequently unloading) with known weights attached to its bottom edge. We find a linear response with no measurable hysteresis up to about 9% linear strain, and extract a Young's modulus of $E \approx 245$ kPa for all the sheets independent of their thickness. The bending rigidity of the sheets is calculated as $B = \frac{Eb^3}{12(1-\nu^2)}$, using $\nu \approx 0.48$ as the Poisson ratio for silicone rubber; for the sheets used in our experiments, B is in the range of 0.4–3.3 μN m.

Spheres of different materials (Delrin, 1.4 g cm^{-3}; borosilicate glass, 2.4 g cm^{-3}; stainless steel, 8.05 g cm^{-3}), with radii in the range 2–8 mm, are released in close proximity to the top of the sheet. The point of release is halfway across the width of the sheet (in the x-direction, Fig. 1) so that the spheres are symmetric with respect to either edge of the sheet. The motion of the spheres is recorded at 30 frames s^{-1} with a camera (Nikon D5100); motion in the x-direction is found to be negligible. All measurements were carried out at an ambient temperature of 22 ± 0.5 °C.

Data availability

The experimental data for the plots within this paper are available from the figshare repository[27]. The same repository contains a movie corresponding to Fig. 1a. Raw image data and other supporting data relevant to this study are available from the authors upon request.

References

46. Cox, R. G. & Brenner, H. The slow motion of a sphere through a viscous fluid towards a plane surface—II small gap widths, including inertial effects. *Chem. Eng. Sci.* **22**, 1753–1777 (1967).